Oximation reaction induced reduced graphene oxide gas sensor for formaldehyde detection

Article (Published Version)

Journal of Saudi Chemical Society (2020) xxx, xxx–xxx

King Saud University

Journal of Saudi Chemical Society

www.ksu.edu.sa
www.sciencedirect.com

ORIGINAL ARTICLE

Oximation reaction induced reduced graphene oxide gas sensor for formaldehyde detection

Lei Zhou [a,d], Rong Qian [a,*], Shangjun Zhuo [a], Qiao Chen [b], Zhaoyin Wen [c], Guorong Li [a]

[a] *National Center for Inorganic Mass Spectrometry in Shanghai, Shanghai Institute of Ceramics, Chinese Academy of Sciences, Shanghai 200050, PR China*
[b] *Department of Chemistry, School of Life Science, University of Sussex, Brighton BN1 9QJ, United Kingdom*
[c] *CAS Key Laboratory of Materials for Energy Conversion, Shanghai Institute of Ceramics, Chinese Academy of Sciences, Shanghai 200050, PR China*
[d] *Center of Materials Science and Optoelectronics Engineering, University of Chinese Academy of Sciences, Beijing 100049, PR China*

Received 24 December 2019; revised 2 February 2020; accepted 10 February 2020

KEYWORDS

Oximation reaction;
Reduced graphene oxide;
Gas sensor;
Formaldehyde;
Selectivity

Abstract High-performance gas sensors can offer great potentials for monitoring and detection of volatile organic compounds (VOCs) in both domestic and industrial environment. In the present work, a new HCHO gas sensor was constructed with reduced graphene oxide (RGO) induced by the oximation reaction. The gas-sensing performance test results suggested that the RGO hydroxylamine hydrochloride (RGO/HA-HCl) sensor presented a high response of 75% at 16 ppm HCHO at room temperature, and a high selectivity for HCHO suffering little interference with high concentrations of volatile organic compounds, including methanol, ethanol, and methylbenzene, dichloromethane and water. Additionally, the RGO/HA-HCl sensor also showed a good long-term stability with RSD of 5.83% for a 15-day continuous sensing test, and the detection limit (DL) could reach 0.023 ppm under ambient conditions. Moreover, the mechanism for the high sensitivity and selectivity of formaldehyde was further established by in-situ gas chromatography mass spectrometry (GC–MS). This work would provide a reliable new HCHO gas sensor which could be used for monitoring and forewarning the emission of HCHO for a better protection and improvement of our environment.

* Corresponding author.
E-mail address: qianrong@mail.sic.ac.cn (R. Qian).
Peer review under responsibility of King Saud University.

ELSEVIER Production and hosting by Elsevier

1. Introduction

HCHO as a common chemical, is extensively used in industrial manufacture for the fabrication of resin, rubber, paper, pesticide and textile and so on [1]. However, HCHO is also a serious toxic pollutant that can cause asthma, cancer, leukemia

https://doi.org/10.1016/j.jscs.2020.02.001
1319-6103 © 2020 The Authors. Published by Elsevier B.V. on behalf of King Saud University.

Please cite this article in press as: L. Zhou et al., Oximation reaction induced reduced graphene oxide gas sensor for formaldehyde detection, Journal of Saudi Chemical Society (2020), https://doi.org/10.1016/j.jscs.2020.02.001

and some other diseases [2]. In 2010, the World Health Organization (WHO) determined an important standard that a maximum allowable indoor HCHO concentration cannot exceed 0.08 ppm [3]. In most cases, it is very difficult for people to be conscious of low concentration of HCHO, thus it is urgent to develop the advanced techniques for the fast detection and early warning of HCHO. In the literatures, various methods have been reported for HCHO detection, such as high performance gas chromatography mass spectrometry [4], polarography [5], phenol reagent method [6], fluorescence [7] and spectrophotometry methods [8] and so on. Although these methods displayed high sensitivity and selectivity of the detection of HCHO, most of them required complicated sample preparation and bulky testing instruments. In contrast, portable, integrated semiconductor gas sensors are undoubtedly a better choice for on-site detecting due to many distinct advantages. These include low cost, facile operation, fast and real-time "detect to warn" which became more effective for mobile applications as internet-connected devices [9,10]. Hence, the practical semiconductor gas sensors have higher commercial potential with wider applications in the future smart environmental monitoring.

Most of the semiconductor gas sensors measure the resistance changes, which offer uninterrupted sensing signals. They are based on the electrons or holes exchange or chemical reactions with chemisorbed oxygen ion (O^-, O^{2-}) on the sensing channel surface of the materials [11]. Semiconducting-metal oxides (SMOs), such as ZnO [12], SnO_2 [13] and CuO [14] have been widely developed for the gas-sensing materials because of their high sensitivity and fast response time [15–17]. In most cases, single and pure components have limited sensitivity and selectivity for specific molecules, due to their nonselective surface electronic interactions of the oxides [18]. Usually, the structural regulation and surface modification are considered effective methods to improve the gas-sensing performance. For instance, Long et al. [19] synthesized 3D hierarchical $ZnCo_2O_4$ microstructure with a low-power microheater for a detection limit of 0.03 ppm HCHO at 300 °C with good long-term stability. Wang et al. [20] fabricated Co-doped In_2O_3 nanorods for a highest response of 23.2 for 10 ppm HCHO at 130 °C. Wan et al. [21] designed In_2O_3@SnO_2 core–shell nanofiber via electrospinning and hydrothermal methods for HCHO detection, with instantaneous response/recovery time (3/3.6 s) for 100 ppm HCHO at 120 °C.

Recently, graphene or derivatives based binary nanocomposites, are promising for detecting trace concentrations of VOCs due to their properties of reducing the sensor operation temperature while maintaining their sensitivity. For instance, Ashraf et al. [22] reported a novel RGO/$ZnWO_3$ HCHO gas sensor for a high response of 21.4% for 10 ppm HCHO at 95 °C with a linear correlation between achieved responses and concentration of target gas (1–10 ppm). Wang et al. [23] synthesized mesoporous ultrathin SnO_2 nanosheets in situ modified by graphene oxide (GO) for a response value (*Ra*/*Rg*) as high as 2275 toward 100 ppm HCHO at 60 °C. Sun et al. [24] adopt a solution-based self-assembly method for synthesis of RGO/$ZnSnO_3$ composites for HCHO detection, with low detection limit of 0.1 ppm HCHO at 103 °C. Li et al. [25] fabricated the RGO/MoS_2 hybrid film for a room-temperature HCHO gas sensor with 4.6% response for 15 ppm HCHO. Song et al. [26] adopt RGO-modified silicon nanowires for synthesis of a core–shell structure for HCHO sensor, which could reach a satisfactory detection limit as low as 0.035 ppm of HCHO. However, despite considerable progress, main challenges including stable daily applications with high selectivity, low DL while operating at room temperature without interference of humidity still remain for ideal HCHO gas sensors.

In the present work, a novel HCHO gas sensor was designed and fabricated based on low cost RGO sheets. In order to improve the sensitivity, an interdigitated electrode configuration was adapted. The selectivity of the sensor was guaranteed by using a porous polyvinylidene difluoride (PVDF) membrane modified with hydroxylamine hydrochloride (HA-HCl) salt. In order to achieve the best sensitivity of HCHO, four types of hydroxylamine salts were compared experimentally. Little interferences with other common VOCs, including ethanol, methanol, toluene, acetonitrile, and isopropanol, were also evaluated at room temperature. The HCl vapor, generated by oximation reaction between HA-HCl and HCHO, was affecting the carrier density of the RGO sheets to provide continuously sensing signals specifically for the selective detection of HCHO. The RGO/HA-HCl sensor achieved a satisfactory detection limit of 0.023 ppm under ambient condition at room temperature with relative humidity (RH) of 39.5%. Although the RGO/HA-HCl sensor is specifically sensitive to HCHO, similar principle can also be applied to design gas sensors for other specific VOCs.

2. Experimental section

2.1. Chemicals and reagents

All the chemicals and reagents used were analytical grade in the experiments. Graphene oxide (GO) was purchased from NanoInnova Technologies SL (Madrid, Spain). The interdigitated electrode (1 cm × 1 cm squared alumina substrate with width of the electrode wire of 90 μm and 5 electrode pairs) was purchased from MECART Sensor Technologies SL (Guangzhou, P. R. China).

2.2. Synthesis of reduce graphene oxide

RGO sheets were synthesized by the chemical reduction method according to the reported procedures [27]. Briefly, with an ultrasonic bath (180 W) for 30 min, GO was dispersed in deionized water (0.1 $mg{\cdot}mL^{-1}$, 10 ml). The 10 mg of L-ascorbic acid (L-AA) was then added into GO dispersion with an ultrasonic bath (180 W) for 2 h. After that, the solution was kept 48 h at 26 °C. The final RGO was rinsed with deionized water several times and dried at 60 °C overnight.

2.3. Materials characterization

The morphologies and microstructures of samples were characterized by field emission scanning electron microscopy (FE-SEM, S-4800N, Hitachi, Japan) and field emission transmission electron microscopy (FE-TEM, JEM-2100F, JEOL, Japan). The phase and crystal structure of samples was obtained by using X-ray diffraction (XRD Rigaku Ultima IV, Japan, 40 KV/20 mA, Cu-Karadiation). The surface com-

Please cite this article in press as: L. Zhou et al., Oximation reaction induced reduced graphene oxide gas sensor for formaldehyde detection, Journal of Saudi Chemical Society (2020), https://doi.org/10.1016/j.jscs.2020.02.001

position samples were characterized by X-ray photoelectron spectrometer (ESCALAB 250, USA). The structural changes of samples were characterized by Raman spectroscopy (RENISHAW in Via Raman Microscope, UK). The oximation reaction product was characterized by gas chromatography mass spectrometry (GC–MS, TSQ 8000, Thermofisher, USA).

2.4. Construction of the RGO/HA-HCl sensor

The diagram of the RGO/HA-HCl sensor was illustrated in Scheme 1, the sensor was fabricated and composed of hydroxylamine salts, porous PVDF membrane, RGO sheets and interdigitated electrode. During the preparation procedure, RGO sheets were dissolved in deionized water with an ultrasonic bath (180 W) for 2 h at room temperature and the suspension (0.1 $mg{\cdot}mL^{-1}$) was sprayed coating on the interdigitated electrode. Then, hydroxylamine hydrochloride ($NH_2OH{\cdot}HCl$) was dissolved in methanol (80 $mg{\cdot}mL^{-1}$) and the solution was dropped on the PVDF membrane (0.2 μm of pore size) that which is suspended over RGO sheets. The porous PVDF membrane was used to build a gas channel for transferring HCl vapor. Furthermore, two spacers with the thickness of 0.2 mm were inserted between RGO and PVDF membrane loaded with hydroxylamine hydrochloride.

2.5. Gas-sensing test system

A gas-sensing test system was designed and illustrated in Scheme 2. It was composed of the sealed gas-sensing chamber, gas feeding tubes and a data acquisition system. The gas-sensing chamber was made by a 100 ml electrolytic cell with gas inlet and outlet. The platinum electrodes were used to connect the sensor electrodes to the resistance measurement equipment, and the data was recorded by Keithley 2701 data acquisition system. The sensitivity (S) of the sensor defined by $[Ro-Rg]/Ro \times 100$ (%), where Ro represents the initial resistance in clean air, while Rg represents the resistance in the presence of VOCs. Dry air was used as carrier gas and salt solutions were used to adjust the humidity of test chamber. Before the gas-sensing test, the RGO/HA-HCl sensor was installed in the gas-sensing chamber. Stable carrier gas flow and desired humidity were maintained until the resistance of the sensor is constant. HCHO at different flow rate, mixed with carrier gas (300 ml/min), was introduced into gas-sensing chamber for test. The RGO/HA-HCl sensor was exposed to analyte gases with a fixed feeding time of 500 sec and a recovery time of 500 sec. The initial resistance of the RGO/HA-HCl sensor was around 30–50 kΩ and the nearly linear I-V relationship suggests the ohmic contacts between RGO and interdigitated electrodes (Fig. S1). All the tests were performance at room temperature.

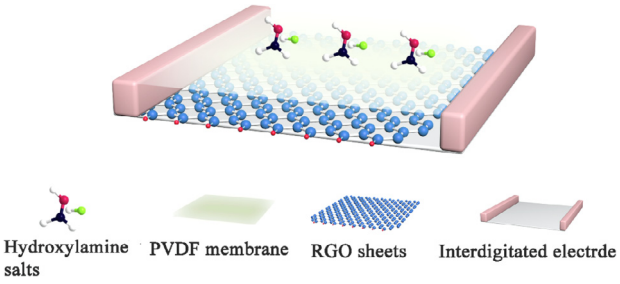

Scheme 1 The diagram of the RGO/HA-HCl sensor.

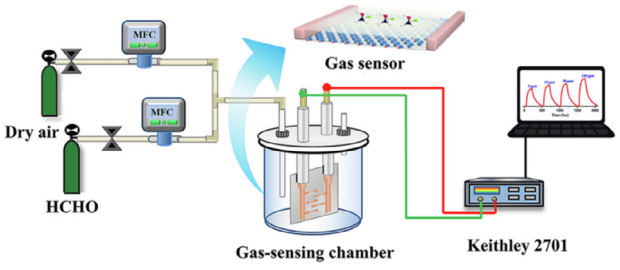

Scheme 2 The diagram of a gas-sensing test system.

3. Results and discussion

3.1. Characterization of materials

The morphologies of GO, RGO sheets and the RGO sheets deposited on the interdigitated electrode were shown in Fig. 1. GO sheet show a uniform wrinkled laminar structure due to a tendency of spontaneously reducing surface energy (Fig. 1a), RGO sheets were homogeneous and displayed a certain texture due to sp^3 character from functionalization [28]. shown in Fig. 1b. The RGO sheets deposited on the interdigitated electrode displays a lot of wrinkles (Fig. 1c), which could be caused by the drying stresses associated with surface tension during the evaporation of solvent [29]. HR-TEM images (Fig. 1d, e) could further reveal detailed structures of the RGO sheets. Fig. 1d indicated that the large RGO sheets were partially overlapping with folds and laminate consistent with our FE-SEM observation. High resolution TEM image in Fig. 1e reveals the graphitic laminar structure in the ordered region, and d spacing of the RGO samples was 0.38 nm. The selected area electron diffraction (SAED) pattern with well-defined diffraction spots (Fig. 1f) illustrated the crystallinity of the reduced GO, which is good agreement with the literature [30].

The crystalline structures of the GO, RGO sheets were identified by XRD. As shown in Fig. 2a, the XRD pattern of the GO (blue curve) is dominated by a strong and sharp peak at $2\theta = 11.7°$ assigned to the (0 0 2) plane. The XRD pattern of RGO (red curve) presents a sharp peak at $2\theta = 24.0°$, as well as a broad peak at higher diffraction angle. The sharp peak gives the interlayer distance of 3.81 Å, which was close to the (0 0 2) diffraction peak of graphite (d-spacing 3.35 Å) [27]. These XRD results shows the distinct differences between RGO and GO due to the exfoliation and reduction of GO and the removing of most of the oxygen-containing groups [31].

The structural changes from GO to RGO sheets were also characterized by the Raman spectra. As reported in the literatures, the G bands (1363 cm^{-1}) was assigned to the E_{2g} mode of sp^2-bonded carbon atoms and D bands (1594 cm^{-1}) was assigned to the symmetry A_{1g} mode [32]. Fig. 2b suggested that the relative intensities ratio of the D bands and G bands (I_D/I_G) increased from 0.76 to 1.09 significantly, which could fur-

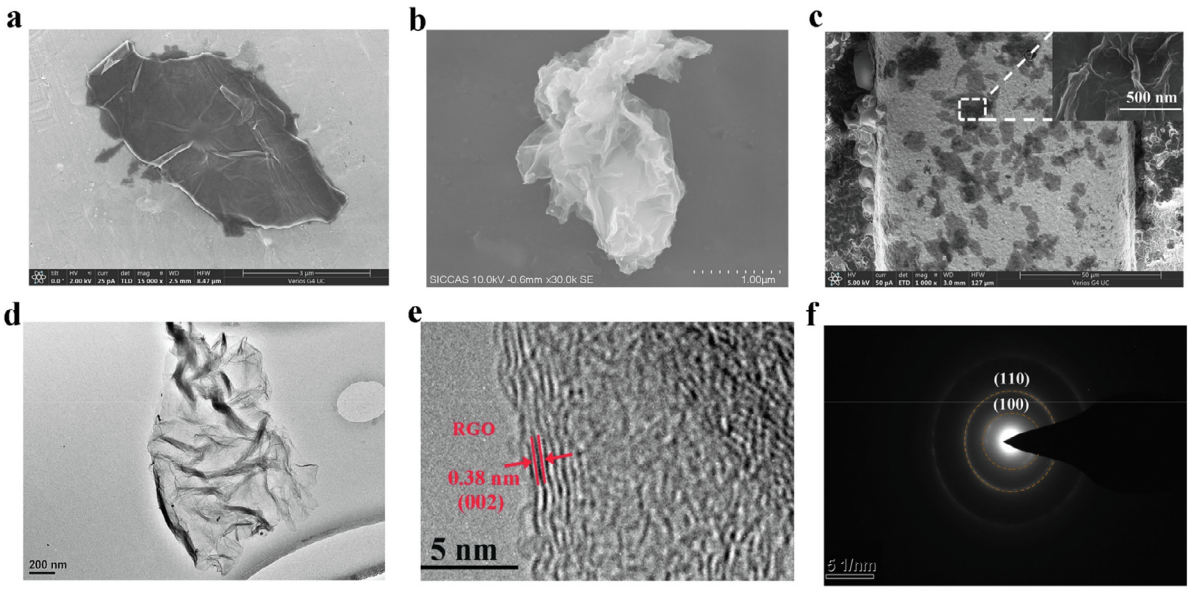

Fig. 1 SEM images of (a) GO sample, (b) RGO sample, (c) RGO sensor. HRTEM images of (d, e) RGO sheets, (f) SAED pattern of RGO sheets.

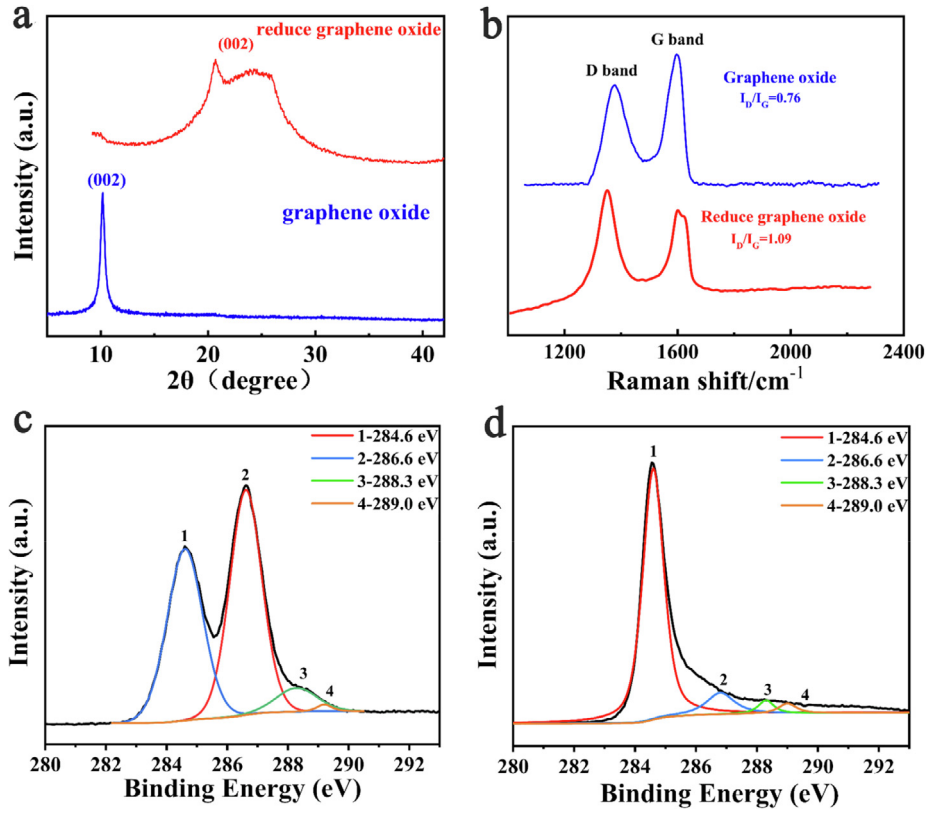

Fig. 2 (a) XRD pattern of GO sheets and the prepared RGO sheets. (b) Raman spectra of the GO sheets and the RGO sheets. (c) High-resolution XPS spectra of C1s for GO sheets. (d) High-resolution XPS spectra of C1s for RGO sheets.

ther confirm that the reduction did take place from GO to RGO.

The reduction of GO was also characterized by X-ray photoelectron spectra (XPS). As shown in Fig. 2c and d, four different peaks at 284.6, 286.6, 288.3 and 289.0 eV were assigned to C=C/C–C, C–O, C=O and C(O)O groups respectively [33]. After reduction, both the peaks associated with C-O, C=O and C(O)O were reduced significantly. These results confirm that the majority of GO was converted to RGO after the reduction reaction. We think the purity of the RGO is crit-

ical for the sensitivity of the sensor, since it can affect noise level of the baseline.

3.2. Investigation of gas-sensing performance

Fig. 3a demonstrates the response of the interdigitated RGO sensor. With hydroxylamine salt modified PVDF membrane, due to the change of response mechanism, the response is much more sensitive. On the other hand, without HA-HCl, the response is almost disappeared. Different types of hydroxylamine, including 1. hydroxylamine hydrochloride (NH_2-OH·HCl), 2. hydroxylamine (NH_2OH), 3. hydroxylamine sulphate ($NH_2OH·H_2SO_4$) and 4. o-benzylhydroxylamine hydrochloride ($NH_2OC_7H_7$·HCl) were compared for their sensitivity to HCHO. Fig. 3b shows that hydroxylamine hydrochloride offers the highest sensitivity for RGO sensor. O-benzylhydroxylamine hydrochloride offers a reduced sensitivity, while hydroxylamine and hydroxylamine sulphate provide little response to HCHO. The reasons for the different sensitivity will be discussed in Section 3.3. Nevertheless, hydroxylamine hydrochloride (NH_2OH·HCl) was selected for the fabrication of the ultrasensitive HCHO gas sensor for further test.

To investigate the selectivity to HCHO, the RGO/HA-HCl sensor was exposed to various VOCs at room temperature. Fig. 4a shows different response curves for four VOCs in comparison to HCHO, including methanol, ethanol, methylbenzene, and dichloromethane. The response to water vapor was also included. The measured response, together with their exposed concentration is shown in Fig. 4b. The selectivity of RGO/HA-HCl sensor for HCHO was 1000 times higher than other five gases, and only the HCHO gives the highest positive response. The response for other VOCs and water vapor are all negative, indicating an increased resistance.

In previous reports, specially designed or chemically modified semiconductors were developed to enhance the sensor selectivity to targeted gas samples [18,34,35]. For example, the anisotropically formed particles provided different pore sizes to offer size selective gas sensors, allowing smaller gas molecule to diffuse towards the sensor surface. To enhance the selectivity, noble metal nanoparticles was used to increase the adsorption energy of analytes [36–38]. While in our present study, the selectivity is controlled by a highly selective reaction between HCHO and HA-HCl through oximation reaction (eq.1), while its sensitivity is enhanced by using low cost and low power consumption, interdigitated electrode configura-

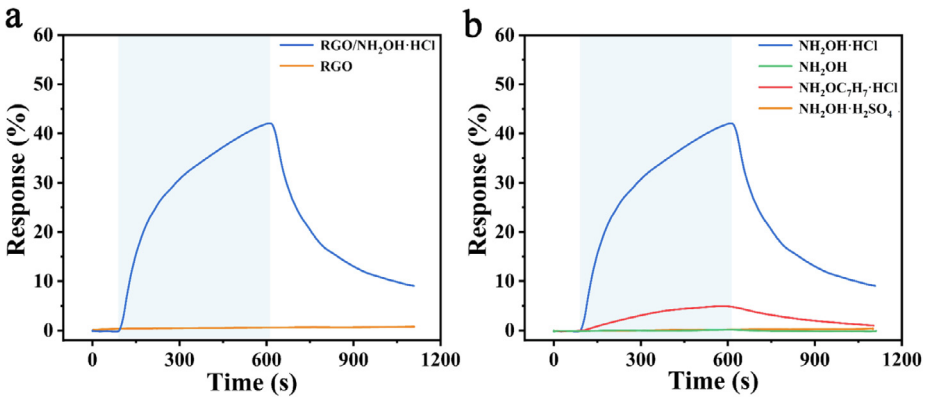

Fig. 3 (a) Gas-sensing properties of the pristine RGO sensor without hydroxylamine salts and RGO/HA-HCl sensor to 8 ppm of HCHO at room temperature, RH of 39.5%. (b) Gas-sensing properties of the RGO sensor with four hydroxylamine salts (1–4) to 8 ppm of HCHO at room temperature, RH of 39.5%.

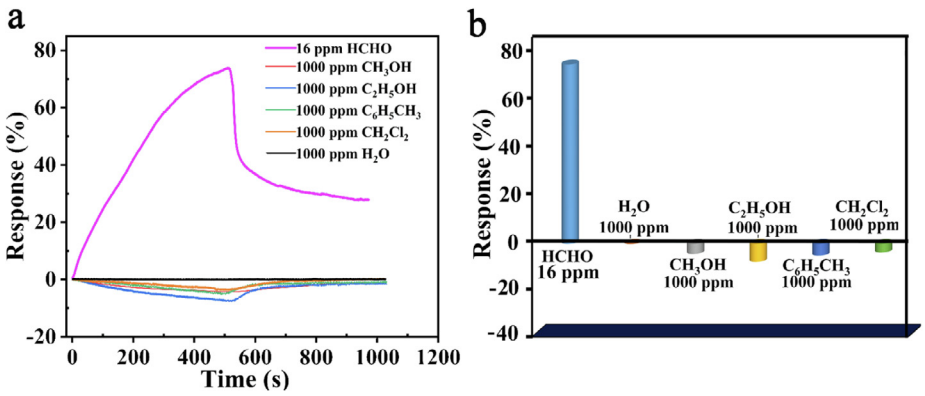

Fig. 4 (a) Gas-sensing properties of response curves for the RGO/HA-HCl sensor to various VOCs gas including formaldehyde, methanol, ethanol, and methylbenzene, dichloromethane and water at room temperature, RH of 39.5%. (b) Selectivity of the RGO/HA-HCl sensor to five VOCs gas and water.

tions. Notably, oximation reactions on the PVDF membranes release hydrochloric acid (HCl). The exposure to the HCl could be responsible for the increases of RGO conductivity. It is worth noting that RGO sheets is sensitive to single-electron oxidant including HCl acids [39]. As a p-type semiconductor, surface modification with strong acid could increase majority charge carrier (hole) density, which increases the conductivity of the RGO. Later, we will confirm this by exposing the sensor with HCl vapor. More important, the oximation reaction is specifically effective to HCHO, which guarantees the unique sensor selectivity to HCHO, even with the high concentration of the interference VOCs. In addition, the high concentration of interference VOCs can swell the RGO sheets or inject electrons, which decreases the conductivity of the RGO sheets.

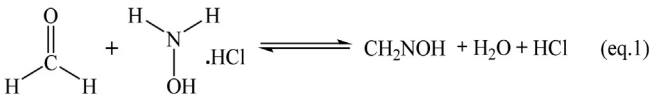

To systematically investigate the sensitivity to HCHO, the RGO/HA-HCl sensor was exposed to an increase of HCHO concentrations varying from 1 ppm to 16 ppm. Fig. 5a suggested that the RGO/HA-HCl sensor presented a maximum response of 75% at 16 ppm HCHO. The response was increased when HCHO is introduced and recovered to its original state after stopping the HCHO gas injection. As expected, the response of the RGO/HA-HCl sensor was gradually increased with an increase of HCHO concentrations. HCHO was introduced to the sensing chamber for 500 sec followed by purging with air. The response curves for RGO/HA-HCl sensor to 16 ppm of HCHO are shown in Fig. S2f. It is suggested that the recovery time was also increased to 1211 s when the concentration of HCHO was increased to 16 ppm. It is interesting to observe the different response curvatures between exposing and purging. The exposing curvature has the signal increases gradually until it reaches a maximum response. This curvature is determined by the diffusion and reaction of HCHO with HA-HCl and the adsorption of HCl on RGO surfaces. However, the purging response curvature seems to show a two steps recovery process. First it is subject to a faster recovery followed by a slower recovery process. We propose that the faster recovery is due to the desorption of surface HCl on RGO, while the slower recovery is due to the desorption of HCl from the bulk RGO with higher desorption energy barrier. Hence, the slow recovery becomes more obvious for higher concentration of HCHO.

Fig. 5b exhibited the linear relationship between gas concentrations and the sensor responses, indicating the reliable responses over the tested concentration range. The 0.39 ppm was the lowest concentration of HCHO detected in this work. The theoretical detection limit (DL) can be calculated using the formula: DL = $3RMS_{noise}$ (root mean square)/slop [40]. In our experiment, the theoretical DL could reach approximately 0.023 ppm, which was much lower than the allowable indoor HCHO concentration of 0.080 ppm.

The stability of the RGO/HA-HCl sensor and its performance at constant exposure is shown in Fig. S3, recording the response at 8 ppm HCHO for 15 days sampled every 3 days. Fig. 6a suggested that the gas response was relatively stable for the detection of HCHO with a relative standard deviation (RSD) of 5.83%. Hence, the RGO sheets surface was not changed significantly with the absorption of HCl vapor. More importantly, the adsorption and desorption of HCl on RGO is probably a reversible process which is responsible for the long-term reliability and stability of the RGO/ HA-HCl sensor.

The influence of humidity on the sensor sensitivity was also investigated in detail (Fig. S4). Fig. 6b exhibited the comparison of response at 8 ppm HCHO with 1.5%, 20.5%, 39.5% and 60.5%. It is interesting that the response of the RGO/ HA-HCl sensor was improved as the relative humidity increased. In contrary, most of the literatures reported that humidity could limit the practical application of P-type semiconductor gas sensors operating at room temperature [41,42]. The present of H_2O molecules would decrease the sensitivity, and sometimes even provided false response. However, our RGO/HA-HCl sensor was allowable to operate at high relative humidity. This could indicate that H_2O molecules help to dissociate HA-HCl, which in turn accelerate the oximation reaction between HCHO and HO-NH_2·HCl. However, the response of the RGO/ HA-HCl sensor decreased when the

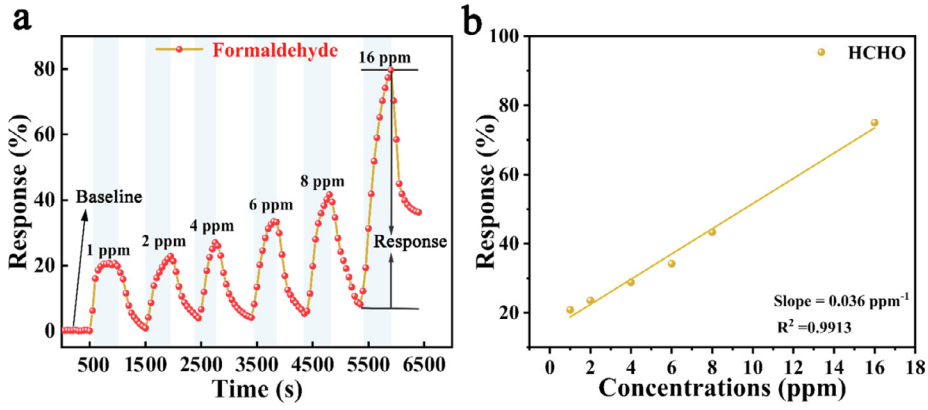

Fig. 5 (a) Gas-sensing properties sensitivity of the RGO/HA-HCl sensor with concentration ranging from 1 to 16 ppm of HCHO at room temperature, RH of 39.5%. (b) The fitting calibration response curve of the RGO/HA-HCl sensor to HCHO at a concentration range of 1–16 ppm.

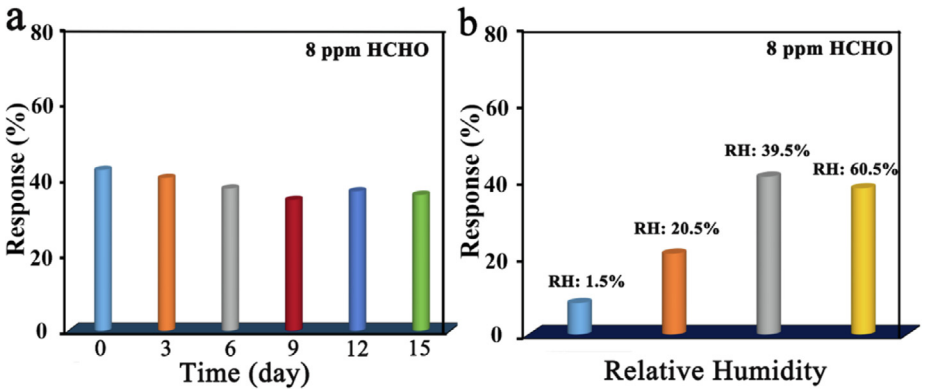

Fig. 6 (a) The long-term stability test of the RGO/HA-HCl sensor for 15 days with an interval of 3 days at 8 ppm of HCHO at room temperature, RH of 39.5%. (b) Gas-sensing properties of the RGO/HA-HCl sensor with different relative humidity (RH = 1.5%, 20.5%, 39.5%, 60.5%) at 8 ppm of HCHO at room temperature.

RH increased from 39.5% to 60.5%. The excessive H_2O molecules can also provide more negative response, such as occupying the surface of the gas-sensitive material and electrons injection. Moreover, compared to the previous Graphene-based HCHO gas sensor (as shown in Table 1), the present RGO/HA-HCl sensor was demonstrated with high gas-sensing performance including high selectivity, sensitivity and a low l detection limit while operating at room temperature without certain relative-humidity HCHO detection.

3.3. Investigation of gas-sensing mechanism

To demonstrate the oximation reaction as the gas-sensing mechanism, an in-situ GC–MS was used for detecting the major oximation reaction, formaldoxime (CH_2NOH, m/z = 45). Fig. 7a indicated that formaldoxime was increased with increasing the HCHO exposure time up to 500 sec, which is consistent with sensor response behavior (Fig. 5a).

After the oximation reaction, HCl vapor is diffused to the RGO sample, which behaves as an electron withdrawing dopant. Hence, the adsorbed HCl will increase the hole density for the p-type RGO. This explains the reduction of RGO resistivity [51,52]. To confirm this mechanism, pure HCl vapor was directly injected into the gas-sensing chamber. Fig. 7b shows that the response of the RGO/HA-HCl sensor had similar behavior as the exposure of HCHO, i.e. the resistance decreased upon HCl vapor exposure. This result confirms that HCl vapor has played an important role in improving both the sensitivity and selectivity of the novel HCHO sensor. This observation also helps to explain the results with different types of hydroxylamine, including 1. hydroxylamine hydrochloride ($NH_2OH{\cdot}HCl$), 2. hydroxylamine (NH_2OH), 3. hydroxylamine sulphate ($NH_2OH{\cdot}H_2SO_4$) and 4. o-benzylhydroxylamine hydrochloride ($NH_2OC_7H_7{\cdot}HCl$). Due to the lack of HCl and the nonvolatile H_2SO_4, hydroxylamine and hydroxylamine sulphate offered very little response to HCHO. Meanwhile, in comparison with o-benzylhydroxylamine hydrochloride, HA-HCl gives higher response signal. This can be understood that HA-HCl has lower energy barrier for the oximation reaction with HCHO.

Based on the above studies, the HCHO gas-sensing mechanism was on RGO/HA-HCl sensor illustrated in Scheme 3. In summary, when the RGO/HA-HCl sensor was exposed to the HCHO, the oximation reaction would release the HCl vapor

Table 1 Comparison of the HCHO gas-sensing performance of the RGO/HA-HCl sensor with previously reported Graphene-based sensors.

Materials	Temperature (°C)	Concentration of HCHO (ppm)	Response	DL (ppm)	Selectivity ratio[a] (S_F/S_H)	RH (%)
RGO/$ZnWO_3$ [22]	95	10	21.4[a]	0.092	5.25	20
RGO/$ZnSnO_3$ [24]	103	10	12.8[a]	0.1	5.5	Dry
RGO/Fe-Doped ZnO [43]	300	10	33[a]	0.016	–	60
GO/SnO_2 [44]	120	100	32[a]	0.5	2.1	40
RGO/SnO_2 [45]	160	100	138[a]	1	3.7	40
RGO/In_2O_3 [46]	225	25	88[a]	–	4.4	53
GO/TiO_2 [47]	RT	0.5	0.64%[b]	0.1	–	Dry
VG/SnO_2 [48]	RT	5	4.6%[b]	0.02	3.4	Dry
RGO/ZnO [49]	RT	45	8%[b]	2	20	Dry
RGO/MoS_2 [25]	RT	15	3%[b]	–	–	Dry
RGO/MoS_2 (visible-light activation) [50]	RT	10	64%[b]	1	3	Dry
RGO/HA-HCl in this work	RT	16	75%[b]	0.023	668	39.5

[a] Response = Ro/Rg.
[b] Response = $|Ro\text{-}Rg|/Ro \times 100$ (%). Selectivity ratio[a] (S_F/S_H) represents the selectivity of the gas sensor between formaldehyde and the interference gas with the highest response. " - " represents that it is not mentioned in the references

Please cite this article in press as: L. Zhou et al., Oximation reaction induced reduced graphene oxide gas sensor for formaldehyde detection, Journal of Saudi Chemical Society (2020), https://doi.org/10.1016/j.jscs.2020.02.001

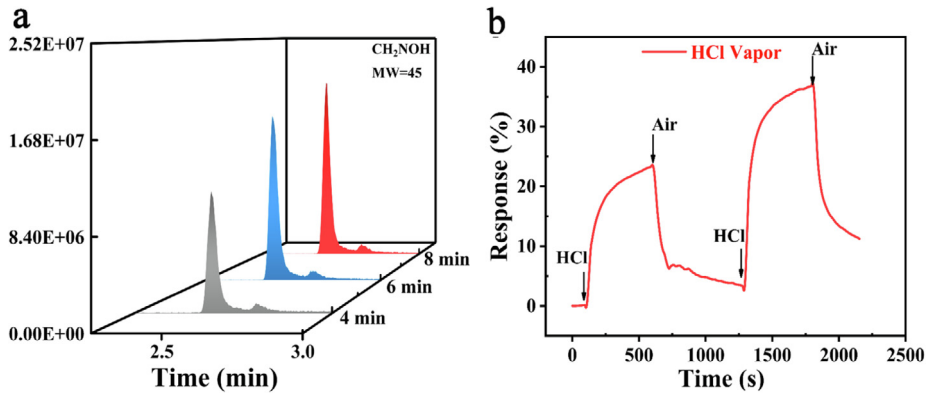

Fig. 7 (a) The GC spectra for the oximation reaction product (CH_2NOH, m/z = 45) at the reaction times of 4 min, 6 min and 8 min respectively. (b) Gas-sensing properties of the RGO/HA-HCl sensor with pure HCl vapor operating at room temperature, RH of 39.5%.

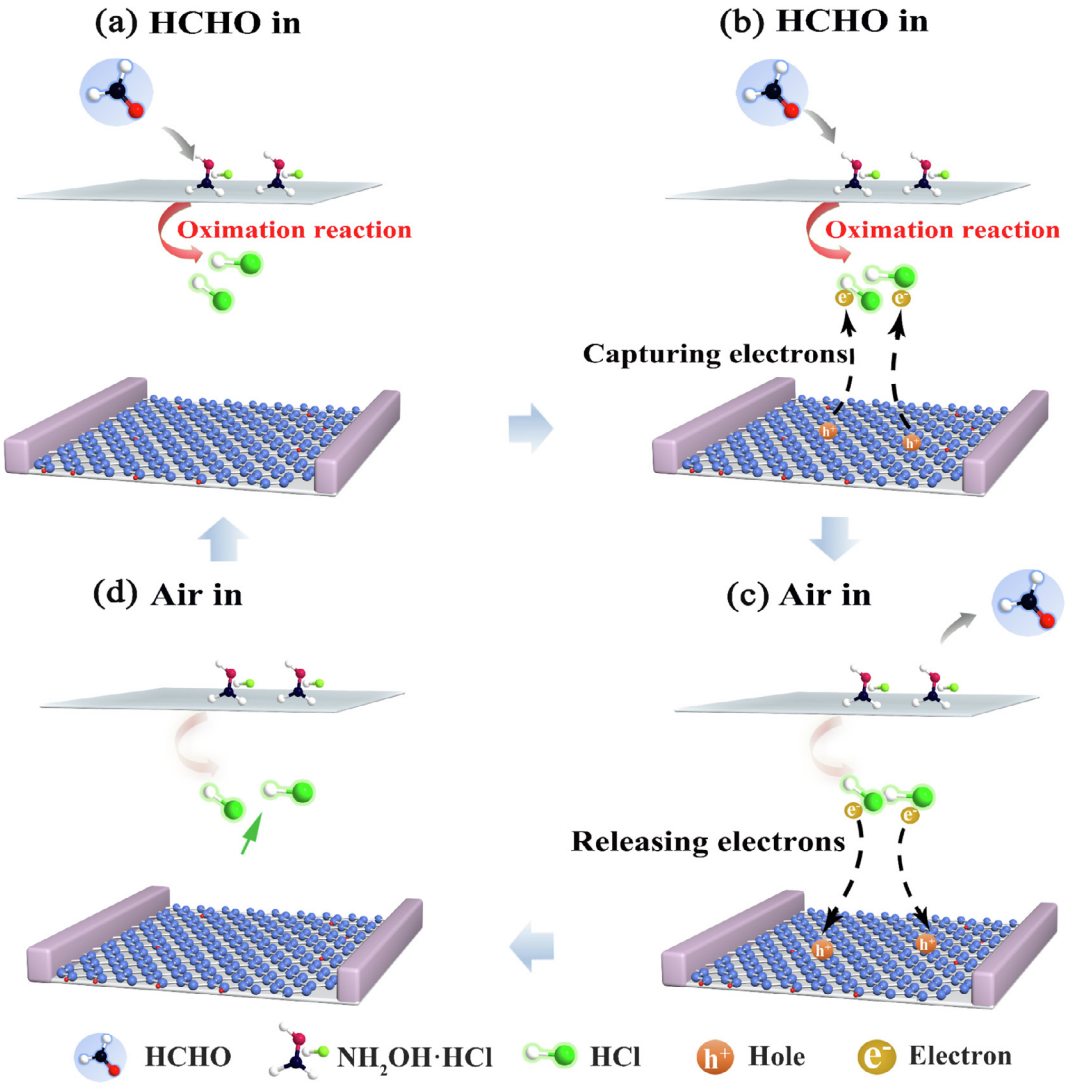

Scheme 3 Schematic illustration of a possible gas-sensing mechanism for the RGO/HA-HCl sensor.

immediately. Subsequently, the released HCl vapor diffuses to the RGO surface to capture electrons from the RGO sheets and leave an equal number of carrier holes on the RGO sheets which decreases the resistance. By purging with air, the adsorbed HCl vapor would desorb from the RGO, which could induce the recombination of holes and electrons leading

to the recovery the resistance of the RGO sheets. During the whole process, the RGO sheets surface served as a catalytic reducing agent, driving the chemical disproportionation of adsorbed dopant layers into charge-transfer complexes which inject majority carriers of electron hole into the 2D carbon lattice [53]. Both surface and intercalated sites were used to adsorb the HCl. However, the internally adsorbed HCl sites has higher desorption energy barrier. This offers two types sensor recovery kinetics: faster surface recovery and slower bulk recovery.

4. Conclusions

Here, a highly sensitive and reliable gas sensor with high selectivity for HCHO was successfully fabricated. The gas sensor is based on interdigitated electrode with RGO sheets and hydroxylamine hydrochloride modified porous PVDF membrane. In addition to the excellent selectivity, the RGO/HA-HCl sensor exhibited ultrahigh sensitivity toward low concentration HCHO with DL of 0.023 ppm. The RGO/HA-HCl sensor showed very little response to high concentrations interferential volatiles including methanol, ethanol, and methylbenzene, dichloromethane and water. Furthermore, these superior sensing properties were achieved under ambient conditions including room temperature and common environment humidity.

The possible mechanism for the high selectivity and sensitivity was further elucidated by GC–MS and the experiment with pure HCl vapor. The results confirmed that oximation reactions taking place on the PVDF membrane would release the HCl vapor to capture the electrons from the RGO sheets to decrease the resistance of the RGO/HA-HCl sensor. Its selectivity towards HCHO is hence guaranteed by the specific reaction oximation and the sensitivity was also enhanced accordingly.

Declaration of competing interest

The authors declare no competing financial interest.

Acknowledgements

The authors greatly acknowledge the financial support by the National Natural Science Foundation of China (Grant 21775156), Intergovernmental International Cooperation Project of Shanghai Science and Technology Commission (Grant 19520712000), and Project of the Technology Center, Shanghai Tobacco (Group) Cooperation (K2018-1-056p).

Appendix A. Supplementary data

Supplementary data to this article can be found online at https://doi.org/10.1016/j.jscs.2020.02.001.

References

[1] X.J. Tang, Y. Bai, A. Duong, M.T. Smith, L.Y. Li, L.P. Zhang, Formaldehyde in China: production, consumption, exposure levels, and health effects, Environ. Int. 35 (2009) 1210–1224.
[2] T. Salthammer, S. Mentese, R. Marutzky, Formaldehyde in the indoor environment, Chem. Rev. 110 (2010) 2536–2572.
[3] Y. Zheng, J. Wang, P. Yao, Formaldehyde sensing properties of electrospun NiO-doped SnO(2) nanofibers, Sens. Actuators B Chem. 156 (2011) 723–730.
[4] J. Luong, X.H. Yang, Y.J. Hua, P.L. Yang, R. Gras, Gas chromatography with in situ catalytic hydrogenolysis and flame ionization detection for the direct measurement of formaldehyde and acetaldehyde in challenging matrices, Anal. Chem. 90 (2018) 13855–13859.
[5] Z.Q. Zhang, H. Zhang, G.F. He, Preconcentration with membrane cell and adsorptive polarographic determination of formaldehyde in air, Talanta 57 (2002) 317–322.
[6] M. Panizza, G. Cerisola, Removal of organic pollutants from industrial wastewater by electrogenerated Fenton's reagent, Water Res. 35 (2001) 3987–3992.
[7] P.P. Li, D. Zhang, Y.C. Zhang, W. Lu, W.Q. Wang, T. Chen, Ultrafast and efficient detection of formaldehyde in aqueous solutions using chitosan-based fluorescent polymers, ACS Sens. 3 (2018) 2394–2401.
[8] Y. Tang, X. Kong, A. Xu, B. Dong, W. Lin, Development of a two-photon fluorescent probe for imaging of endogenous formaldehyde in living tissues, Angew. Chem. Int. Ed. 55 (2016) 3356–3359.
[9] M.X. Zhang, C.H. Zhao, H.M. Gong, G.Q. Niu, F. Wang, Porous gan submicron rods for gas sensor with high sensitivity and excellent stability at high temperature, ACS Appl. Mater. Interfaces 11 (2019) 33124–33131.
[10] G.J. Li, X.H. Wang, L.M. Yan, Y. Wang, Z.Y. Zhang, J.Q. Xu, PdPt bimetal-functionalized SnO_2 nanosheets: controllable synthesis and its dual selectivity for detection of carbon monoxide and methane, ACS Appl. Mater. Interfaces 11 (2019) 26116–26126.
[11] S.-Y. Cho, D. Jang, H. Kang, H.-J. Koh, J. Choi, H.-T. Jung, Ten nanometer scale WO_3/CuO heterojunction nanochannel for an ultrasensitive chemical sensor, Anal. Chem. 91 (2019) 6850–6858.
[12] M.W. Ahn, K.S. Park, J.H. Heo, J.G. Park, D.W. Kim, K.J. Choi, J.H. Lee, S.H. Hong, Gas sensing properties of defect-controlled ZnO-nanowire gas sensor, Appl. Phys. Lett. 93 (2008).
[13] S. Das, V. Jayaraman, SnO_2: a comprehensive review on structures and gas sensors, Prog. Mater Sci. 66 (2014) 112–255.
[14] X.B. Hu, Z.G. Zhu, Z.H. Li, L.L. Xie, Y.H. Wu, L.Y. Zheng, Heterostructure of CuO microspheres modified with $CuFe_2O_4$ nanoparticles for highly sensitive H_2S gas sensor, Sens. Actuators B Chem. 264 (2018) 139–149.
[15] N. Barsan, U. Weimar, Conduction model of metal oxide gas sensors, J. Electroceram. 7 (2001) 143–167.
[16] H.J. Kim, J.H. Lee, Highly sensitive and selective gas sensors using p-type oxide semiconductors: overview, Sens. Actuators B Chem. 192 (2014) 607–627.
[17] D.H. Lee, S.K. Kang, Y. Pak, N. Lim, R. Lee, Y. Kumaresan, S. Lee, C. Lee, M.-H. Ham, G.Y. Jung, Transfer of preheat-treated SnO_2 via a sacrificial bridge-type ZnO layer for ethanol gas sensor, Sens. Actuators B Chem. 255 (2018) 70–77.
[18] K. Suematsu, K. Watanabe, A. Tou, Y. Sun, K. Shimanoe, Ultraselective toluene-gas sensor: nanosized gold loaded on zinc oxide nanoparticles, Anal. Chem. 90 (2018) 1959–1966.
[19] H. Long, A. Harley-Trochimczyk, S. Cheng, H. Hu, W.S. Chi, A. Rao, C. Carraro, T. Shi, Z. Tang, R. Maboudian, Nanowire-assembled hierarchical $ZnCo_2O_4$ microstructure integrated with a low-power microheater for highly sensitive formaldehyde detection, ACS Appl. Mater. Interfaces 8 (2016) 31764–31771.
[20] Z. Wang, C. Hou, Q. De, F. Gu, D. Han, One-step synthesis of Co-doped In_2O_3 nanorods for high response of formaldehyde sensor at low temperature, ACS Sens. 3 (2018) 468–475.

[21] K. Wan, D. Wang, F. Wang, H. Li, J. Xu, X. Wang, J. Yang, Hierarchical In_2O_3@SnO_2 core-shell nanofiber for high efficiency formaldehyde detection, ACS Appl. Mater. Interfaces 11 (2019) 45214–45225.
[22] M.A. Ashraf, Z. Liu, W. Peng, Z. Parsaee, Design, preparation and evaluation of a high performance sensor for formaldehyde based on a novel hybride nonocomposite $ZnWO_3$/rGO, Anal. Chim. Acta 1051 (2019) 120–128.
[23] D. Wang, L. Tian, H. Li, K. Wan, X. Yu, P. Wang, A. Chen, X. Wang, J. Yang, Mesoporous ultrathin SnO_2 nanosheets in situ modified by graphene oxide for extraordinary formaldehyde detection at low temperatures, ACS Appl. Mater. Interfaces 11 (2019) 12808–12818.
[24] J.H. Sun, S.L. Bai, Y. Tian, Y.H. Zhao, N. Han, R.X. Luo, D. Q. Li, A.F. Chen, Hybridization of $ZnSnO_3$ and rGO for improvement of formaldehyde sensing properties, Sens. Actuators B Chem. 257 (2018) 29–36.
[25] X. Li, J. Wang, D. Xie, J. Xu, Y. Xia, W. Li, L. Xiang, Z. Li, S. Xu, S. Komarneni, Flexible room-temperature formaldehyde sensors based on rGO film and rGo/MoS_2 hybrid film, Nanotechnology 28 (2017).
[26] L.F. Song, L.Q. Luo, Y. Xi, J.J. Song, Y. Wang, L.P. Yang, A. Q. Wang, Y.F. Chen, N. Han, F.Y. Wang, Reduced graphene oxide-coated Si nanowires for highly sensitive and selective detection of indoor formaldehyde, Nanoscale Res. Lett. 14 (2019).
[27] J. Zhang, H. Yang, G. Shen, P. Cheng, J. Zhang, S. Guo, Reduction of graphene oxide via L-ascorbic acid, Chem. Commun. 46 (2010) 1112–1114.
[28] I. Jung, D. Dikin, S. Park, W. Cai, S.L. Mielke, R.S. Ruoff, Effect of water vapor on electrical properties of individual reduced graphene oxide sheets, J. Mater. Chem. C 112 (2008) 20264–20268.
[29] Y. Chen, F. Guo, A. Jachak, S.-P. Kim, D. Datta, J. Liu, I. Kulaots, C. Vaslet, H.D. Jang, J. Huang, A. Kane, V.B. Shenoy, R.H. Hurt, Aerosol synthesis of cargo-filled graphene nanosacks, Nano Lett. 12 (2012) 1996–2002.
[30] G. Wang, J. Yang, J. Park, X. Gou, B. Wang, H. Liu, J. Yao, Facile synthesis and characterization of graphene nanosheets, J. Mater. Chem. C 112 (2008) 8192–8195.
[31] R.F. Albers, R.A. Bini, J.B. Souza Jr., D.T. Machado, L.C. Varanda, A general one-pot synthetic strategy to reduced graphene oxide (rGO) and rGO-nanoparticle hybrid materials, Carbon 143 (2019) 73–84.
[32] S. Stankovich, D.A. Dikin, R.D. Piner, K.A. Kohlhaas, A. Kleinhammes, Y. Jia, Y. Wu, S.T. Nguyen, R.S. Ruoff, Synthesis of graphene-based nanosheets via chemical reduction of exfoliated graphite oxide, Carbon 45 (2007) 1558–1565.
[33] A. Kovtun, D. Jones, S. Dell'Elce, E. Treossi, A. Liscio, V. Palermo, Accurate chemical analysis of oxygenated graphene-based materials using X-ray photoelectron spectroscopy, Carbon 143 (2019) 268–275.
[34] Y. Liu, Y. Jiao, Z. Zhang, F. Qu, A. Umar, X. Wu, Hierarchical SnO_2 Nanostructures made of intermingled ultrathin nanosheets for environmental remediation, smart gas sensor, and supercapacitor applications, ACS Appl. Mater. Interfaces 6 (2014) 2174–2184.
[35] W.Y. Chen, C.C. Yen, S.C. Xue, H.Y. Wang, L.A. Stanciu, Surface functionalization of layered molybdenum disulfide for the selective detection of volatile organic compounds at room temperature, ACS Appl. Mater. Interfaces 11 (2019) 34135–34143.
[36] J.-H. Kim, A. Mirzaei, H.W. Kim, S.S. Kim, Extremely sensitive and selective sub-ppm CO detection by the synergistic effect of Au nanoparticles and core-shell nanowires, Sens. Actuators B Chem. 249 (2017) 177–188.
[37] X. Liu, J. Zhang, L. Wang, T. Yang, X. Guo, S. Wu, S. Wang, 3D hierarchically porous ZnO structures and their functionalization by Au nanoparticles for gas sensors, J. Mater. Chem. 21 (2011) 349–356.
[38] K. Suematsu, Y. Shin, Z. Hua, K. Yoshida, M. Yuasa, T. Kida, K. Shimanoe, Nanoparticle cluster gas sensor: controlled clustering of SnO_2 nanoparticles for highly sensitive toluene detection, ACS Appl. Mater. Interfaces 6 (2014) 5319–5326.
[39] S. Ishihara, J. Labuta, T. Nakanishi, T. Tanaka, H. Kataura, Amperometric detection of sub-ppm formaldehyde using single-walled carbon nanotubes and hydroxylamines: a referenced chemiresistive system, ACS Sens. 2 (2017) 1405–1409.
[40] J. Li, Y.J. Lu, Q. Ye, M. Cinke, J. Han, M. Meyyappan, Carbon nanotube sensors for gas and organic vapor detection, Nano Lett. 3 (2003) 929–933.
[41] N. Joshi, T. Hayasaka, Y.M. Liu, H.L. Liu, O.N. Oliveira, L.W. Lin, A review on chemiresistive room temperature gas sensors based on metal oxide nanostructures, graphene and 2D transition metal dichalcogenides, Microchim. Acta 185 (2018) 16.
[42] M. Sinha, R. Mahapatra, B. Mondal, T. Maruyama, R. Ghosh, Ultrafast and reversible gas-sensing properties of ZnO nanowire arrays grown by hydrothermal technique, J. Mater. Chem. C 120 (2016) 3019–3025.
[43] W. Guo, B. Zhao, Q. Zhou, Y. He, Z. Wang, N. Radacsi, Fe-doped ZnO/reduced graphene oxide nanocomposite with synergic enhanced gas sensing performance for the effective detection of formaldehyde, Acs Omega 4 (2019) 10252–10262.
[44] D. Wang, M. Zhang, Z. Chen, H. Li, A. Chen, X. Wang, J. Yang, Enhanced formaldehyde sensing properties of hollow SnO_2 nanofibers by graphene oxide, Sens. Actuators B Chem. 250 (2017) 533–542.
[45] X. Rong, D. Chen, G. Qu, T. Li, R. Zhang, J. Sun, Effects of graphene on the microstructures of SnO_2@rGO nanocomposites and their formaldehyde-sensing performance, Sens. Actuators B Chem. 269 (2018) 223–237.
[46] R.K. Mishra, G. Murali, T.H. Kim, J.H. Kim, Y.J. Lim, B.S. Kim, P.P. Sahay, S.H. Lee, Nanocube In_2O_3@rGO heterostructure based gas sensor for acetone and formaldehyde detection, Rsc Adv. 7 (2017) 38714–38724.
[47] Z. Ye, H. Tai, T. Xie, Z. Yuan, C. Liu, Y. Jiang, Room temperature formaldehyde sensor with enhanced performance based on reduced graphene oxide/titanium dioxide, Sens. Actuators B Chem. 223 (2016) 149–156.
[48] Z. Bo, M. Yuan, S. Mao, X. Chen, J. Yan, K. Cen, Decoration of vertical graphene with tin dioxide nanoparticles for highly sensitive room temperature formaldehyde sensing, Sens. Actuators B Chem. 256 (2018) 1011–1020.
[49] X. Li, J. Wang, D. Xie, J. Xu, R. Dai, L. Xiang, H. Zhu, Y. Jiang, Reduced graphene oxide/hierarchical flower-like zinc oxide hybrid films for room temperature formaldehyde detection, Sens. Actuators B Chem. 221 (2015) 1290–1298.
[50] J. Wang, H. Deng, X. Li, C. Yang, Y. Xia, Visible-light photocatalysis enhanced room-temperature formaldehyde gas sensing by MoS_2/rGO hybrids, Sens. Actuators B Chem. 304 (2020).
[51] A. Kasry, M.A. Kuroda, G.J. Martyna, G.S. Tulevski, A.A. Bol, Chemical doping of large-area stacked graphene films for use as transparent, conducting electrodes, ACS Nano 4 (2010) 3839–3844.
[52] B. Chandra, A. Afzali, N. Khare, M.M. El-Ashry, G.S. Tulevski, Stable charge-transfer doping of transparent single-walled carbon nanotube films, Chem. Mater. 22 (2010) 5179–5183.
[53] R.A. Nistor, D.M. Newns, G.J. Martyna, The role of chemistry in graphene doping for carbon-based electronics, ACS Nano 5 (2011) 3096–3103.

Please cite this article in press as: L. Zhou et al., Oximation reaction induced reduced graphene oxide gas sensor for formaldehyde detection, Journal of Saudi Chemical Society (2020), https://doi.org/10.1016/j.jscs.2020.02.001